ACS APPLIED MATERIALS & INTERFACES

Research Article

www.acsami.org

New Yellow-Emitting Nitride Phosphor $SrAlSi_4N_7:Ce^{3+}$ and Important Role of Excessive AlN in Material Synthesis

Liangliang Zhang,[†,‡] Jiahua Zhang,*[,†] Xia Zhang,[†] Zhendong Hao,[†] Haifeng Zhao,[†] and Yongshi Luo[†]

[†]State Key Laboratory of Luminescence and Applications, Changchun Institute of Optics, Fine Mechanics and Physics, Chinese Academy of Sciences, 3888 Eastern South Lake Road, Changchun 130033, China

[‡]University of Chinese Academy of Sciences, Beijing, 100039, China

ABSTRACT: Synthesis and luminescent properties of Ce^{3+}-doped $SrAlSi_4N_7$ yellow-emitting phosphor are reported. In comparison with YAG: Ce^{3+}, the phosphor exhibits smaller thermal quenching and a broader emission band centering at 555 nm with a bandwidth as large as 115 nm, being suitable for fabricating high color rendering white LED. It is observed in material synthesis that intense luminescence can be achieved only in case of excessive AlN in the raw materials. The role of the excessive AlN is studied. The mechanism for existence of edge-sharing $[AlN_4]$ tetrahedral, which is unreasonable according to the aluminum avoidance principle, is discussed in detail.

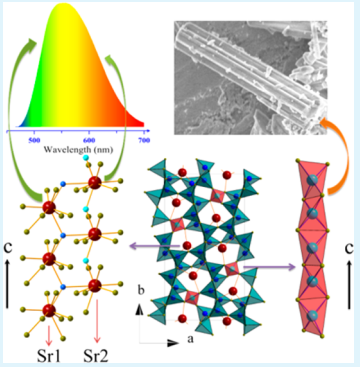

KEYWORDS: *nitridosilicate, phosphor, luminescent property, crystal chemistry, preferred orientation, excessive AlN*

INTRODUCTION

The most widespread commercial strategy to achieve white light-emitting diode (WLED) is using a blue LED chip to excite yellow-emitting YAG:Ce^{3+} phosphor.[1] The color rendering index (CRI) of such a WLED is low (<80)[2] because of deficiency of red fluorescent component in YAG:Ce^{3+}. One of the solutions to the problem is to blend a red phosphor with the yellow one. However, some drawbacks such as fluorescence reabsorption, non-uniformity of luminescence, and time dependent shift of color point arise[3] simultaneously. An ideal solution is to broaden the emission band of single yellow phosphor so as to enrich the red component. In turn, the color rendering[4] is improved without the drawbacks of phosphor blend. Thus, to find a yellow phosphor with an emission band broader than YAG:Ce^{3+} (100 nm) is our interested topic.

$SrAlSi_4N_7$-based phosphor drew our attention because Eu^{2+}-doped $SrAlSi_4N_7$ exhibits an extreme broad emission band. The full width at half-maximum (FWHM) of $SrAlSi_4N_7:Eu^{2+}$ is 116 nm,[5] wider than that of $M_2Si_5N_8:Eu^{2+}$ (M = Ca, Sr, Ba),[6] $CaAlSiN_3:Eu^{2+}$[7] and YAG:Ce^{3+}. Unfortunately, $SrAlSi_4N_7:Eu^{2+}$ is a red emitting phosphor rather than a yellow one, and won't realize white light when coupled with a blue LED chip. According to P. Dorenbos's study,[8] emission of Ce^{3+} always shows considerable blue-shift compared with Eu^{2+} at the same site in the same compound. Therefore observation of a broad yellow emission band in Ce^{3+}-doped $SrAlSi_4N_7$ is expected.

The characteristic of broad emission in $SrAlSi_4N_7:Eu^{2+}$ should be mainly related to $SrAlSi_4N_7$ crystal structure.[5] $SrAlSi_4N_7$ belongs to orthorhombic crystal system, the same as $Sr_2Si_5N_8$ and $CaAlSiN_3$. However, $SrAlSi_4N_7$ contains spatial infinite chains of edge-sharing $[AlN_4]$ tetrahedra running along [0 0 1] in the lattice.[9] Such an edge-sharing type is really unreasonable.[10] Two Al sites locate in the [AlN4] chains and are both coordinated with N1, N2, N4, and N8 atoms. The electrostatic valency sum of N1 is 2.5 which show about 17% divergence from the valence of N atom. Such a divergence excesses the critical value to keep a stable compound. N2, N4, and N8 atoms also show the same situation. A new explanation is, therefore, required.

In synthesis progress, excessive AlN in raw materials was necessary to achieve pure $SrAlSi_4N_7$ phase.[5,9] Similar phenomenon is also observed in the present work. However, the influence of the excessive AlN on formation and luminescence of $SrAlSi_4N_7$-based phosphor is still unknown. Thus further investigation is of importance for better understanding the role of excessive AlN, as was emphasized by J. Ruan.[5]

In this paper, we report synthesis and luminescent properties of a new yellow-emitting Ce^{3+}-doped $SrAlSi_4N_7$ phosphor. Significantly, it shows an emission band broader than YAG:Ce^{3+}, being beneficial for higher CRI. The role of excessive AlN in material synthesis and luminescent properties of $SrAlSi_4N_7:Ce^{3+}$ is studied. The mechanism for existence of edge-sharing [AlN4] tetrahedra is discussed in detail based on bond valence sum calculation and experimentally observed preferred orientation of $SrAlSi_4N_7:Ce^{3+}$ crystals.

Received: July 2, 2013
Accepted: November 20, 2013
Published: November 20, 2013

EXPERIMENTIAL DETAILS

Synthesis. Undoped and Ce-doped $SrAlSi_4N_7$ were synthesized by employing carbothermal reduction and nitridation (CRN) method. Appropriate amounts of $SrCO_3$ (99.99%), α-Si_3N_4 (98%), AlN (99.9%), and CeO_2 (99.99%) were weighted as starting materials according to nominal composition. Fine graphite powder (99.9%) was used as carbon source with amount of 150−250 mol% of Sr atoms. The raw materials were fully grounded in an agate mortar and pressed into a graphite crucible. Then the crucible was positioned in a horizontal tube furnace and fired at 1600 °C with a heating rate of 3 °C/min for 10 h under N_2 gas flow of 0.8 L/min.

Characterization. Powder X-ray diffraction (XRD) patterns were collected by using Cu Kα radiation (λ = 1.54056 Å) on a Bruker D8 Focus diffractometer, operating at 40 kV and 40 mA. The XRD data were collected in range of 5−80° with step size of 0.02° and count time of 3 s/step. Powder diffraction indexing was performed by Dicvol06 program.[11] Cell and spacegroup assignment was performed by Chekcell program. Rietveld refinement was carried out with GSAS program package.[12] The scale factor, zero shift, background, and cell parameters were refined. The diffraction peak positioned at 2θ degree of 35.4°, which is the strongest peak of the standard XRD pattern, is employed for the calculation of 2θ migration and FWHM in the following discussion.

The photoluminescence (PL), photoluminescence excitation (PLE), and diffuse reflectance (DR) spectra were measured by using HITACHI F-4500 spectrometer equipped with a 150 W xenon lamp. Both the excitation and emission slits were set at 2.5 nm. $BaSO_4$ white plate was used as the standard reference for reflection measurement. Response function of the system was determined by using a calibration halogen lamp and rhodamine B solution. The optical properties of white LED were measured by using a micro fiber spectrometer (Ocean Optics, USB4000).

The morphology and elementary composition were investigated by using a field emission scanning electron microscopy (FE-SEM, Hitachi, S-4800) equipped with an energy dispersive spectrometer (EDS). Electron beam conditions were an acceleration voltage of 25 kV and a beam diameter <100 nm. All measurements were corrected for detector dead time, instrumental drift and X-ray back-ground. High-resolution transmission electron microscopy (HRTEM) images were obtained on a JEOL-2100 microscope with an accelerating voltage of 200 kV. The decay time was measured by FL920 fluorimeter (Edinburgh Instruments, Livingston, U.K.) equipped with a hydrogen lamp (nF900). The excitation wavelength is 450 nm with a pulse time of 1 ns.

Diffuse reflectance infrared Fourier transform (DRIFT) spectroscopy was measured by a Fourier transform infrared spectrometer (BIO-RAD, FTS3000, U.S.A.). All the samples were prediluted by KBr and the weight ratio of sample and KBr was 1:10. The temperature-dependent photoluminescence spectrum was carried out on F-4500 spectrometer with an external heater under excitation at 450 nm. A type E thermocouple made up of a positive chromel wire and a negative constantan wire was used to measure the temperature. A type CN76000 process controller (OMEGA) was used to control the heating rate at 1.5 °C/min.

RESULTS AND DISSCUSSION

Luminescence. Ce^{3+}-doped $SrAlSi_4N_7$ is of bright green-yellow body color similar to commercial YAG:Ce^{3+} phosphor. Figure 1 is the DR, PL, and PLE spectra of $SrAlSi_4N_7$:0.05Ce^{3+}.

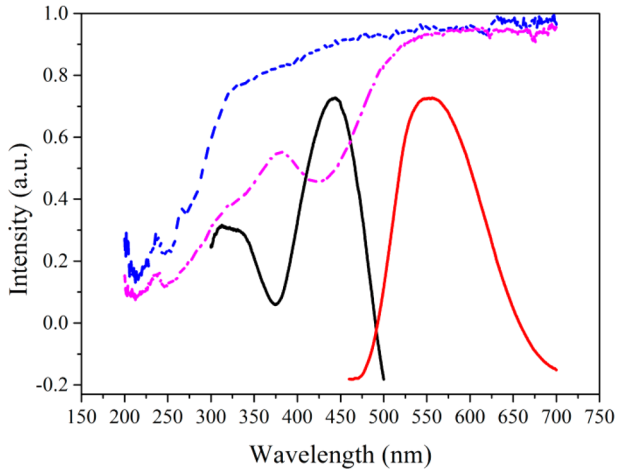

Figure 1. PLE spectrum monitor 555 nm emission (black solid line) and PL spectrum excited by 450 nm (red solid line) of $SrAlSi_4N_7$:0.05Ce^{3+}, DR spectrum of undoped (blue dash line) and Ce-doped SrAlSi4N7 (pink dash dot line).

The reflection spectrum of Ce^{3+}-doped $SrAlSi_4N_7$ shows a strong absorption band accompanied with a weak one covering from near UV to blue, which is absent for undoped $SrAlSi_4N_7$ host. The emission spectrum of $SrAlSi_4N_7$:0.05Ce^{3+} shows a broad yellow band centering at 555 nm with FWHM of ~115 nm which is broader than YAG:Ce^{3+} (centering at 525 nm, FWHM of 100 nm).[13] The excitation spectrum of the yellow emission exhibits a strong band centering at 443 nm and a weak one at 316 nm, which coincides with the DR spectrum. The emission and excitation bands should be ascribed to the transition between the lowest lying 5d state and the ground state of Ce^{3+}.

The excitation spectrum can be decomposed into four Gaussian subbands centering at 32680, 29762, 23256, and 21692 cm^{-1}, respectively. Among the four subbands, 21692 cm^{-1} is assumed to be the band edge of 5d energy level. This is in accordance with P. Dorenbos's empirical rule that the lowest 5d state can be estimated at 80−85% intensity of the first maximum excitation peak.[14] 10Dq,[15] the difference between barycenter of T_{2g} and E_g, is 8747 cm^{-1}. Center of gravity of 5d energy level, estimated by averaging the four excitation subbands, is 26848 cm^{-1}. Compared with Ce^{3+} in YAG,[16] barycenter of Ce^{3+} in $SrAlSi_4N_7$ is ~9800 cm^{-1} lower and 10Dq is ~9300 cm^{-1} narrower. This indicates that redshift of Ce^{3+} emission in $SrAlSi_4N_7$ is mainly ascribed to the nephelauxetic effect while in YAG is mostly caused by strong crystal field.

The temperature-dependent luminescent spectra of $SrAlSi_4N_7$:Ce^{3+} are shown in Figure 2. With increasing temperature, the PL intensities decrease while the peak positions almost keep still. $SrAlSi_4N_7$:Ce^{3+} shows lower quenching temperature compared with YAG:Ce^{3+}, as displayed in top-right corner of Figure 2. The intensity at 150 °C decreases to 78.7% of the initial intensity. The activation energy is estimated by the equation

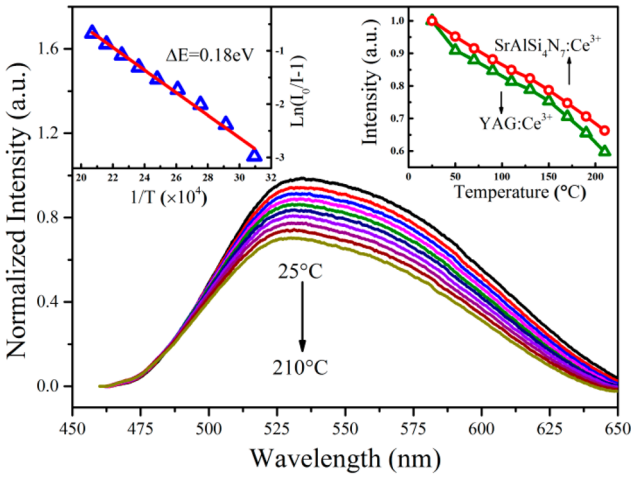

Figure 2. Temperature-dependent luminescent spectra of $SrAlSi_4N_7:Ce^{3+}$ from 25 to 210 °C.

$$I(T) = \frac{I_0}{1 + Re^{-\Delta E/k_b T}}$$

where I_0 is the initial intensity, $I(T)$ is the intensity at temperature T, R is a constant, ΔE is the activation energy, and k_b is Boltzmann's constant. As shown in top-left corner of Figure 2, ΔE for $SrAlSi_4N_7:Ce^{3+}$ is 0.18 eV which equals that of $Ca_3ScSi_3O_{12}:Ce^{3+}$.[17]

Fluorescence decay curves of $SrAlSi_4N_7:0.05Ce^{3+}$ measured by monitoring 540 and 600 nm are shown in Figure 3. The

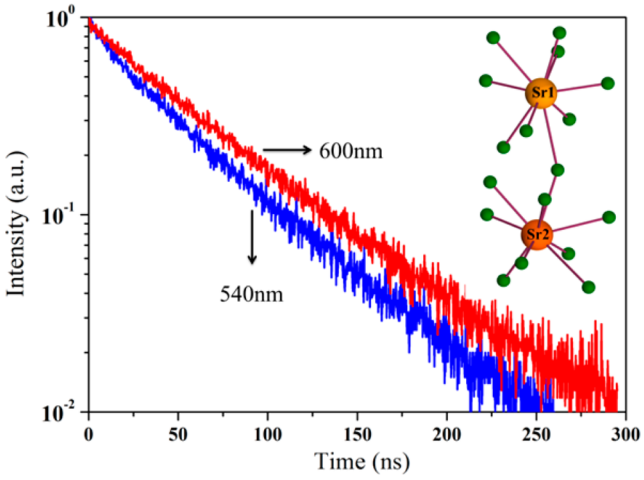

Figure 3. Decay curves of $SrAlSi_4N_7:0.05Ce^{3+}$ monitoring 540 and 600 nm, respectively.

decay curves show different decay times. The decay time monitoring 540 nm is 43.3 ns, while that monitoring 600 nm is 54.2 ns. This implies that the broad emission band of $SrAlSi_4N_7:Ce^{3+}$ is originated from overlap of two Ce^{3+} centers located at two Sr sites in $SrAlSi_4N_7$ lattice. Since the structure of nitridosilicates show a larger flexibility compared with oxosilicates,[18] the coordination numbers of Sr are easily to be mistaken in nitridosilicates. For example, In $Sr_2Si_5N_8$, two Sr sites were initially considered to be sixfold and sevenfold respectively.[19] Afterward, they were considered to be 8 and 10 coordinated, respectively.[20] Finally, they were proved to be both 10 by K. Sohn.[21] An examination of Sr surroundings in $SrAlSi_4N_7$ shows that coordination number of Sr1 and Sr2 are both 9, as shown in upper-right corner of Figure 3, rather than previously reported 6 and 8. The average distances of Sr1−N and Sr2−N are calculated to be 2.89 and 2.91 Å, respectively. According to crystal field theory, the similar interatomic distances of Sr−N and the same coordination number make two luminescence centers spectrally undistinguishable.

White LED is fabricated by combining single $SrAlSi_4N_7:0.05Ce^{3+}$ phosphor with blue InGaN LED (450 nm) chip. Emission spectrum of the WLED is shown in Figure 4.

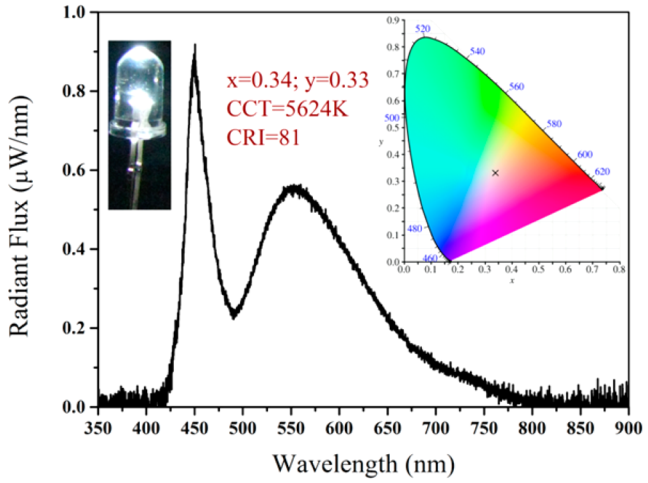

Figure 4. Emission spectrum of WLED achieved by using blue InGaN LED (450 nm) and $SrAlSi_4N_7:0.05Ce^{3+}$ phosphor.

The emission spectrum yields a white light with CRI of 81 and correlated color temperature (CCT) of 5624 K. This indicates that broad emission property endow $SrAlSi_4N_7:Ce^{3+}$ with obvious improvement of color rendering property. However, the luminous efficacy of the WLED is only 12 lm/W. This is ascribed to the residue carbon in phosphor which is a common issue for CRN method. According to our experiments, $SrAlSi_4N_7:Ce^{3+}$ shows almost the same emission intensity as $SrAlSi_4N_7:Eu^{2+}$ synthesized by CRN method. As matter of fact, emission intensity of $SrAlSi_4N_7:Eu^{2+}$ synthesized by nitrogen gas pressure method[5] is ~126% of $YAG:Ce^{3+}$. Thus improvement of synthesis method is necessary to increase the performance of $SrAlSi_4N_7:Ce^{3+}$ phosphor.

Preferred orientation. One can find that intensity distribution of the XRD pattern is quite different from the standard $SrAlSi_4N_7$ phase, as shown in Figure 5a. Diffraction peak at $2\theta = 31.7°$ is the strongest instead of the one at 35.4° which should be the strongest suggested by the standard card. Indexing of powder diffraction lines of undoped $SrAlSi_4N_7$ is performed. The calculation revels that orthorhombic crystal system is the best solution with factor of quality $M(20) = 64.7$ and $F(20) = 114.1$. Spacegroup determination is performed subsequently based on the indexing result. $Pna2_1$ is assigned as the best solution with cell parameters of $a = 11.681$ Å, $b = 21.397$ Å, $c = 4.964$ Å, $\alpha = \beta = \gamma = 90°$, which are close to previously reported results of single crystal structure ($a = 11.742$ Å, $b = 21.391$ Å, $c = 4.966$ Å, $\alpha = \beta = \gamma = 90°$). This reveals that Bragg positions of our $SrAlSi_4N_7$ sample are the same as the standard pattern while the intensity distribution is different. This phenomenon is ascribed to the anisotropic growth of $SrAlSi_4N_7$ crystalline supported by the needle-like crystalline particles in Figure 5b. A further Rietveld refinement is carried out afterwards. The preferred orientation is

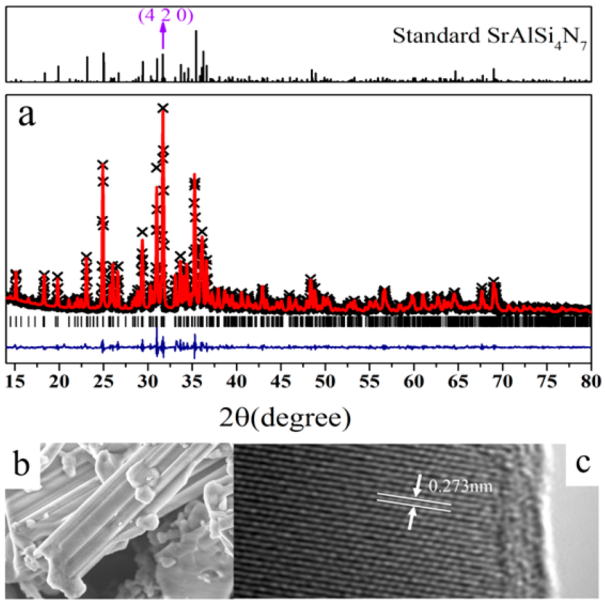

Figure 5. Rietveld refinement plot (a) of undoped SrAlSi4N7 sample. Observed (cross), calculated (line), and difference profile (bottom line) of the XRD pattern are plotted in the same range. Bragg peak positions are shown as vertical bars. Morphology (b) and HRTEM image (c) of the sample.

successfully corrected by using spherical harmonics function and *R*-factors, R_p and R_{wp}, are converged to 3.25% and 4.35% respectively, as shown in Figure 5a.

As is mentioned before, infinite chains of edge-sharing [AlN4] tetrahedra in $SrAlSi_4N_7$ lattice is really unreasonable. Thus, bond valence sum (BVS) calculations are carried out to analyze the chain of edge-sharing [AlN4] tetrahedra with Bond_Str program.[22] However, no big divergence between BVS and valence is observed, as shown in Table 1. The Bond

Table 1. Bond Valence Sum (BVS) Calculation Result

	N1	N2	N4	N8
bond valence sums	2.939	3.055	3.177	3.106
divergence from valence (%)	2.031	1.827	5.859	3.536

valence method has taken experimental Al−N bond length into consideration. Single bond-valence will increase with shortening interatomic distance. Average Al1−N and Al2−N distances in $SrAlSi_4N_7$ are 1.7960 and 1.7491 Å respectively, shorter than theoretical Al−N distance (1.8964 Å). This indicates that [AlN_4] tetrahedra realize edge-sharing connection type by shortening Al−N distance. However, such a connection type isn't the most stable configuration. Shortened Al−N distance and edge-sharing connection type will reduce the interatomic distance of two neighbor Al^{3+} atoms and increase the electrostatic repulsive force between them. According to Pawling's third rule, this effect will increase the instability of the structure. Single-point energy of three [AlN_4] tetrahedra with vertex-sharing and edge-sharing connection types are calculated to be −2300 and −2835 eV respectively, which implies the metastability of edge-sharing [AlN_4] tetrahedra. Thus the metastability is responsible for the anisotropy growth of $SrAlSi_4N_7$ crystalline. As shown in Figure 5a, the intensity of diffraction peak with Miller index of (4 2 0) is extremely high which indicates the preferred growth of (4 2 0) crystal face. This can also be proved by the HRTEM image in Figure 5c, the interplanar d spacing is measured to be 0.273 nm, corresponding to the (4 2 0) plane (d = 0.282 nm). It can be proved that the preferred orientation is perpendicular to the infinite chains of edge-sharing [AlN_4] ([0 0 1] direction).

Summaries of the connection type of [AlN4] tetrahedra in some nitridoalumosilicates are shown in Table 2. Among the

Table 2. Connection Type of [AlN_4] Tetrahedra in Already Known Nitridoalumosilicates

compounds	connection type
$Ca_5Si_2Al_2N_8$[23]	edge-sharing [AlN_4] tetrahedra pair
$Ca_4SiAl_3N_7$[23]	edge-sharing [AlN_4] tetrahedra pair
$SrAlSi_4N_7$[9]	edge-sharing [AlN_4] tetrahedra chain
$Ba_2AlSi_5N_9$[24]	edge-sharing [AlN_4] tetrahedra pair (Si and Al sits not distinguished)
$La_{17}Si_9Al_4N_{33}$[25]	bridging nitrogen atom N[4]
$CaAlSiN_3$[26]	random Al/Si distribution

five nitridoalumosilicates, three contain edge-sharing [AlN_4] tetrahedra pair, one contains [AlN_4] tetrahedra connected by bridging nitrogen atom N[4] and the rest $CaAlSiN_3$ shows a random Al/Si distribution. Another connection type of [AlN4] tetrahedra in nitridoalumosilicates is bridging N[4] atom. Calculation of BVS on aluminum nitride which contains typical N[4] bridging shows that BVS of N is 3.032 (1.07% divergence from valence). The average Al−N distance in AlN is 1.8926 Å and approaches the theoretical value (1.8964 Å). This indicates that N[4] bridging also satisfies electrostatic valency principle. Thus, two [AlN_4] tetrahedra can be connected by edge-sharing or N[4] bridging in nitridoalumosilicates. This conclusion is useful for the determination of new structures from X-ray diffraction since Si and Al sites are difficult to be separated as a consequence of similar atomic form factors.

Effects of excessive AlN. It is normally observed that $SrAlSi_4N_7:Ce^{3+}$ exhibits weak luminescence as stoichiometric amount of AlN is added in raw materials. Strangely, the phosphor emits intense luminescence as excessive AlN is added in raw materials. To understand the origin, Samples with stoichiometric ratio $Sr_{0.95}AlSi_4N_7{\cdot}x$AlN:$0.05Ce^{3+}$ are synthesized with x mol excessive AlN added in raw material. Figure 6 is the XRD patterns of samples with various x. When x = 0, there is an impurity peak at 2θ = 20.5° (marked as *) which is ascribed to Si_3N_4 impurity phase. The Si_3N_4 phase disappears when $x \geq 0.5$. The strongest peak at 2θ = 31.7° (marked as ●) is ascribed to the result of preferred orientation as is discussed above.

Comparing the standard AlN pattern with standard $SrAlSi_4N_7$, one can find that diffraction peaks of AlN are coincided with part of $SrAlSi_4N_7$. As shown in Figure 6, intensities of diffraction peaks at 2θ = 33.2°, 36.1°, and 37.9° (marked as ♦), which belong to both $SrAlSi_4N_7$ and AlN, increase gradually with increasing x. This implies that the pre-added excessive AlN remains in the final product. Infrared absorption spectrum is introduced to show the relative quantity of the remained AlN. AlN powder exhibits two absorption bands at 1300−1350 cm^{-1} ascribed to the overtone of Al−N stretching vibrations and one absorption band at 1400−1450 cm^{-1} due to different stretching vibrations of Al−N. As shown in Figure 7, characteristic absorptions of AlN increase gradually with larger x. $SrAlSi_4N_7$ coexists with large amount of AlN without forming new products.

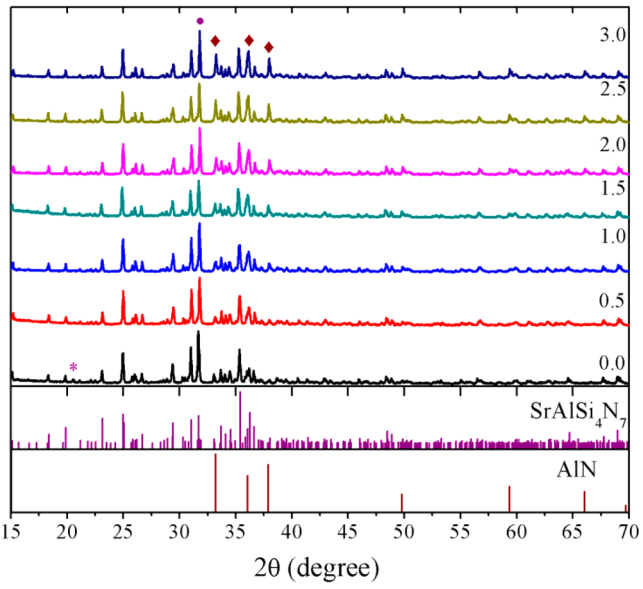

Figure 6. XRD pattern of $Sr_{0.95}AlSi_4N_7{\cdot}x$AlN:0.05$Ce^{3+}$ samples (* represents Si3N4 phase, ● represents the preferred orientation peak, ♦ represents AlN phase).

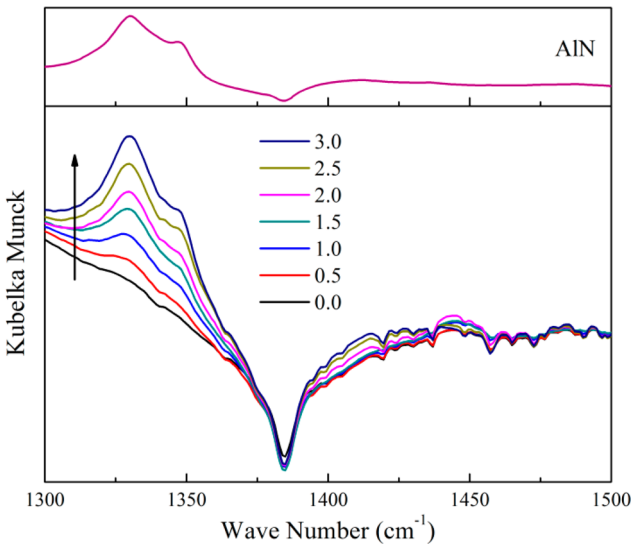

Figure 7. DRIFT spectra of $Sr_{0.95}AlSi_4N_7{\cdot}x$AlN:0.05$Ce^{3+}$ samples.

However, not all of the excessive AlN is remained, Al atoms also enter $SrAlSi_4N_7$ lattice. As shown in Figure 8a, diffraction peaks move to lower 2θ degree with increasing x. This implies the incorporation of larger atoms into $SrAlSi_4N_7$ lattice. The radius of Al^{3+} (0.39 Å, CN=4) is larger than Si^{4+} (0.26 Å, CN = 4) and smaller than Sr^{2+} (1.31 Å, CN = 9). Thus Al^{3+} atom is suggested to substitute for Si^{4+}. As shown in Figure 8b, the PL peaks also move to shorter wavelength. According to the charge cloud attraction effect,[27] replacement of Si^{4+} by larger Al^{3+} results in less attraction to electron cloud of the adjacent nitrogen ions, and then increases the covalency of Ce^{3+} surroundings. This effect will lower the centroid of 5d level and lead to red-shift of the emission. This is obviously conflict with the blue-shift in Figure 8b. Thus we suppose that O^{2-} substitutes for N^{3-} to offer charge compensation for Al^{3+} replacing Si^{4+}. This is because Al−O and Si−N show similar bond length and identical charge. Replacement of Si−N by Al−

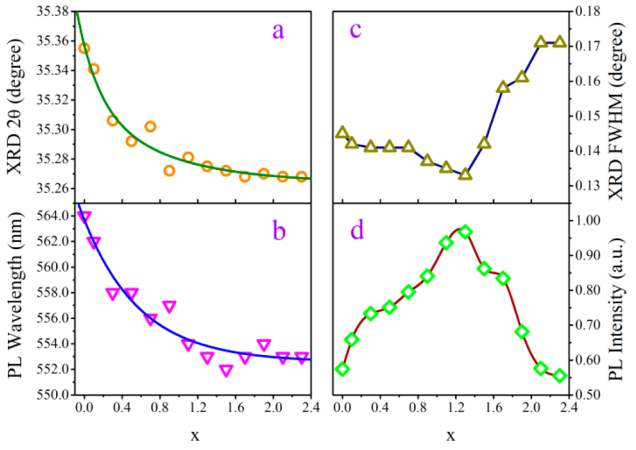

Figure 8. Shift of diffraction peaks (a) and variation of FWHM (c) of the XRD patterns, variation of emission wavelength (b) and intensity (d) of PL of $Sr_{0.95}AlSi_4N_7{\cdot}x$AlN:0.05$Ce^{3+}$ samples.

O is common in nitride and oxynitride, for example, $Y_2Si_3O_3N_3 \rightarrow Y_2Si_{3-x}Al_xO_{3+x}N_{3-x}$[28] with $0 \le x \le 0.6$ and $Ca_5Si_2Al_2N_8 \rightarrow Ca_5Si_{2-x}Al_{2+x}O_xN_{8-x}$[23] with $0 \le x \le 0.6$. Substitution of N^{3-} by more electronegative O^{2-} decreases the degree of covalent bonding and raises the centroid of 5d level according to the nephelauxetic effect.

Elementary composition of the samples is measured by EDS. X-ray radiation of N is absorbed effectively by the matrix[23] and this will lead to big uncertainties of element count. However the EDS result can still offer relative elements quantity. Energy dispersive X-ray spectroscopies of $Sr_{0.95}AlSi_4N_7{\cdot}x$AlN:0.05$Ce^{3+}$ are shown in Figure 9. The spectra are normalized by Kα line of

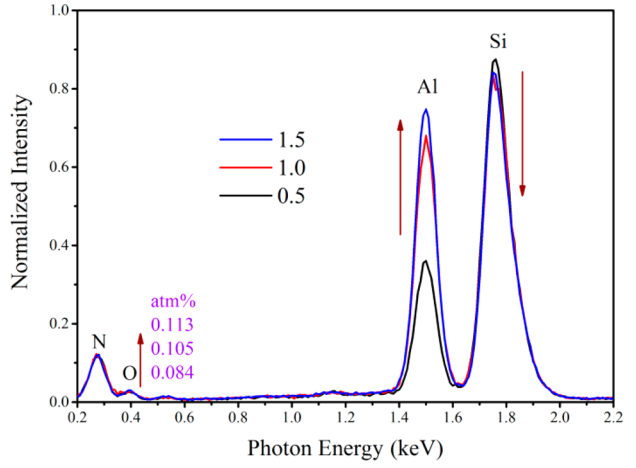

Figure 9. Energy dispersive X-ray spectroscopy of $Sr_{0.95}AlSi_4N_7{\cdot}x$AlN:0.05$Ce^{3+}$ with increasing x.

Sr atom. The concentrations of O and Al atoms increase while that of Si decreases with increasing x. This is in accordance with the assumption that Al−O substitutes for Si−N.

The remained AlN is not just an impurity. It is found that PL intensities of $Sr_{0.95}AlSi_4N_7{\cdot}x$AlN:0.05$Ce^{3+}$ increase with increasing AlN content, as shown in Figure 8d. Simultaneously, FWHM of diffraction peaks decrease as shown in Figure 8c. The intensities become maximum with 1.3 mol excessive AlN while FWHM reach the minimum. Since the DR spectra in Figure 10 show almost unchanged absorbance, the variation of PL intensity isn't relevant to solid solubility of Ce^{3+} in

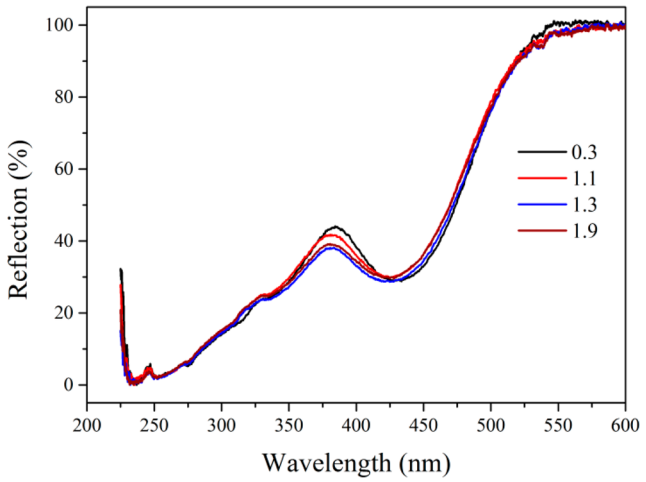

Figure 10. DR spectra of $Sr_{0.95}AlSi_4N_7{\cdot}xAlN{:}0.05Ce^{3+}$ samples.

$SrAlSi_4N_7$. Thus the reduced XRD FWHM means better crystallization of $SrAlSi_4N_7$ crystalline. These results indicate that less AlN is fatal to the synthesis of $SrAlSi_4N_7$, while excessive AlN is beneficial to pure $SrAlSi_4N_7$. However, excessive AlN will introduce O^{2-} resulting from substitution of Si−N by Al−O.

Since there are Al−O substituting for Si−N, we design samples: $Sr_{0.95}Al_{1+y}Si_{4-y}N_{7-y}O_y{:}0.05Ce^{3+}$ with excessive AlN and deficient Si_3N_4 in raw materials. The excessive y mol Al^{3+} is hoped to substitute for y mol Si^{4+}, and simultaneously y mol O^{2-} to substitute for y mol N^{3-} for charge compensation.

Figure 11 shows the shift of diffraction peaks of sample $Sr_{0.95}Al_{1+y}Si_{4-y}N_{7-y}O_y{:}0.05Ce^{3+}$. The positions of diffraction peaks remain unchanged when $y < 0.1$, and move to lower 2θ degree with increasing y from 0.1 up to 0.3. When y is further increased, the peaks no longer move. When $y < 0.1$, Si_3N_4 impurity phase is detected and signal of the phase becomes weaker with increasing y. Pure $SrAlSi_4N_7$ phase can only be achieved when $0.1 \le y \le 0.3$. The shift of XRD peaks when $0.1 \le y \le 0.3$ is the result of a larger Al^{3+} substituting for a smaller Si^{4+} as is discussed earlier. However, such a shift needs less excessive AlN (up to 0.3) in $Sr_{0.95}Al_{1+y}Si_{4-y}N_{7-y}O_y{:}0.05Ce^{3+}$ than that (up to 1.7) in $Sr_{0.95}AlSi_4N_7{\cdot}xAlN{:}0.05Ce^{3+}$. This indicates that Al substituting for Si is more efficient in $Sr_{0.95}Al_{1+y}Si_{4-y}N_{7-y}O_y{:}0.05Ce^{3+}$ samples due to Si vacancy is designed. As y is larger than 0.3, AlN impurity phase is detected followed by little movement of XRD peaks. This means the substitution of Al for Si is saturated.

When $y < 0.1$, although Si_3N_4/AlN in raw materials is less than stoichiometric ratio of 4/3, Si_3N_4 impurity phase still remains. On the contrary, the excessive AlN added in raw materials neither remains in final product nor enters $SrAlSi_4N_7$ lattice. AlN is inferred to be expended on oxidation because its oxidation temperature[29] is only 700°C. As a result, Si_3N_4 is remained.

Covering method is performed to reduce the oxidation of AlN in sintering progress. After being well mixed, raw materials are put into a carbon crucible and compacted. Then, a thin layer of granular activated carbon with a diameter of 0.5 mm is covered upon the raw materials. At last, a layer of AlN powder is covered upon the carbon. After sintering, the three-layer construction is well kept and the bottom layer is $SrAlSi_4N_7{:}Ce^{3+}$ phosphor. This improvement effectively reduces the oxidation of AlN in raw materials and the required excessive AlN is decreased from 8 mol % (least required excessive AlN in raw materials of sample without covering method) to 4 mol % for achieving pure $SrAlSi_4N_7$, as shown in Figure 12.

Another improvement is achieved by using a mechanical vacuum pump to vacuumize the furnace tube before heating. With this progress, the graphite is decreased from 250 to 130 mol% of Sr in raw materials. There are two O sources in the furnace: residual O_2 and O^{2-} derived from SrO. This

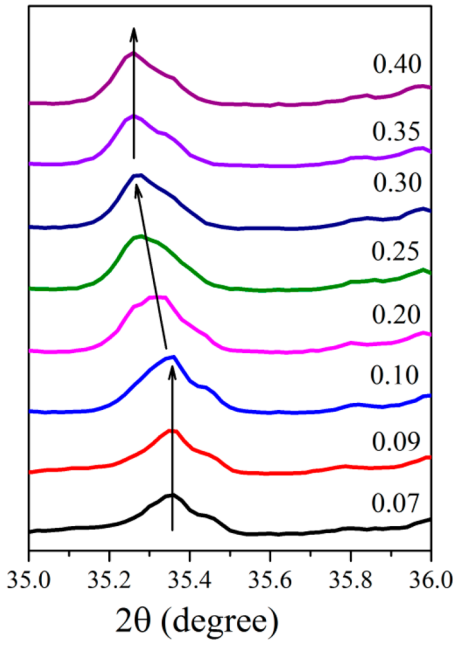

Figure 11. Shift of diffraction peaks (2θ = 35.4°) of $Sr_{0.95}Al_{1+y}Si_{4-y}N_{7-y}O_y{:}0.05Ce^{3+}$ samples.

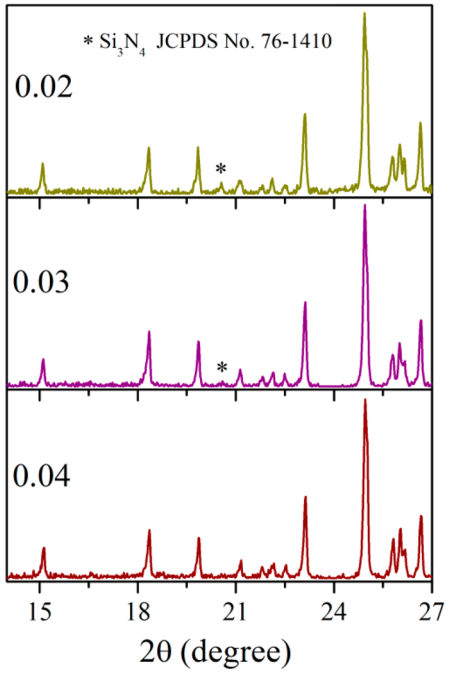

Figure 12. XRD pattern of $SrAlSi_4N_7{:}Ce^{3+}$ synthesized by covering method with different excessive AlN in raw materials.

phenomenon demonstrates that residual O_2 plays a major role in the oxidation of AlN.

Figure 13 shows the emission spectra of $Sr_{0.95}Al_{1+y}Si_{4-y}N_{7-y}O_y$:0.05$Ce^{3+}$ samples. With increasing y,

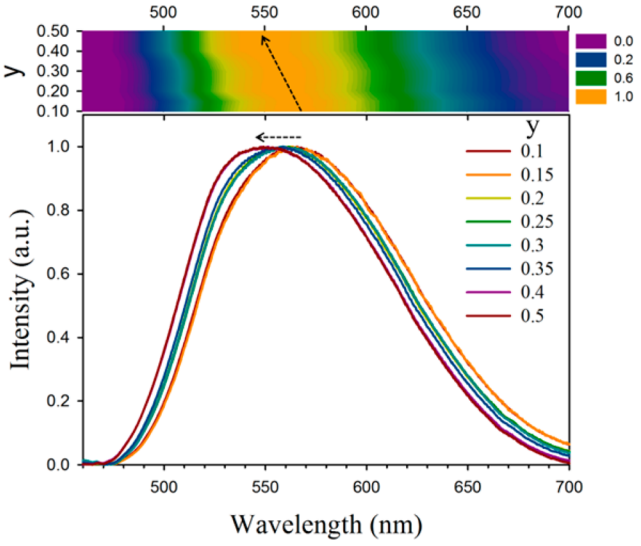

Figure 13. Emission spectra of $Sr_{0.95}Al_{1+y}Si_{4-y}N_{7-y}O_y$:0.05$Ce^{3+}$ samples with various y.

blue-shift of emission from 564 to 550 nm occurs. As discussed earlier, the blue shift is ascribed to O^{2-} substituting for N^{3-}. According to our previous study on nitridation of $Ca_3Sc_2Si_3O_2$,[30] the substitution of N by O has little effect on Bragg positions. Similar phenomenon is also reported by KS. Sohn et, al. when nitriding Sr_2SiO_4.[31] Thus the shift of XRD peaks in Figure 11 reflects the progress of Al^{3+} substituting for Si^{4+} while the movement of PL wavelength in Figure 13 reflects the progress of O^{2-} substituting for N^{3-}. The simultaneous movement of PL wavelength and diffraction peaks is accordant with the assumption that Al−O substituting for Si−N.

CONCLUSIONS

(1) The broad emission property endows $SrAlSi_4N_7$:Ce^{3+} with obvious improvement of color rendering property. There are two Sr sites in $SrAlSi_4N_7$ lattice. Coordination numbers of both Sr sites are 9. Average Sr1−N and Sr2−N distances are 2.89 and 2.91 Å, respectively. $SrAlSi_4N_7$:Ce^{3+} appears a broad emission band due to a spectral overlap of the two luminescence centers. (2) Indexing and spacegroup determination of XRD patterns reveal the preferred orientation of $SrAlSi_4N_7$ crystalline. Bound valence sum (BVS) calculation is introduced to show the rationality of the infinite chains of edge-sharing [AlN4] tetrahedra. However, such a connection type reduces the stability of $SrAlSi_4N_7$ lattice. The metastability of edge-sharing [AlN4] tetrahedra is responsible for the preferred orientation. (3) With increasing excessive AlN in raw materials, $SrAlSi_4N_7$:Ce^{3+} shows better luminescence property. Al^{3+} substituting for Si^{4+} is provided with charge compensation by O^{2-} substituting for N^{3-}, as result of which, blue-shift of PL occurs. Since AlN is proved to be oxidated by residual O_2, covering method is introduced to decrease the least excessive AlN required in raw materials from 8 to 4 mol %.

AUTHOR INFORMATION

Corresponding Author

*E-mail: zhangjh@ciomp.ac.cn.

Notes

The authors declare no competing financial interest.

ACKNOWLEDGMENTS

This work is financially supported by the National Natural Science Foundation of China (10834006, 51172226, 61275055, 11274007) and the Natural Science Foundation of Jilin province (201205024).

REFERENCES

(1) Huang, C.; Chiu, Y.; Yeh, Y.; Chan, T.; Chen, T. *ACS Appl. Mater. Interfaces* **2012**, *4*, 6661−6668.
(2) Li, X.; Dudai, J. D.; Liu, F.; Howe, J. Y.; Zhang, J.; Wang, X. J.; Gu, Z.; Sun, C.; Meltzer, R. S.; Pan, Z. *Light: Sci. Appl.* **2013**, *2*, 1−8.
(3) Liu, Y.; Zhang, X.; Hao, Z.; Luo, Y.; Wang, X.; Zhang, J. *J. Mater. Chem.* **2011**, *21*, 16379−16384.
(4) Thornton, W. A. *J. Opt. Soc. Am.* **1971**, *61*, 1155−1163.
(5) Ruan, J.; Xie, R. J.; Hirosaki, N.; Takeda, T. *J. Am. Ceram. Soc.* **2011**, *94*, 536−542.
(6) Li, Y. Q.; Steen, J. E. J.; Krevel, J. W. H.; Botty, G.; Delsing, A. C. A.; DiSalvo, F. J.; With, G.; Hintzen, H. T. *J. Alloys Compd.* **2006**, *417*, 273−279.
(7) Uheda, K.; Hirosaki, N.; Yamamoto, Y.; Naito, A.; Nakajima, T.; Yamamoto, H. *Electrochem. Solid-State Lett.* **2006**, *9*, H22−H25.
(8) Oorenbos, P. *J. Phys.: Condens. Matter.* **2003**, *15*, 4797−4807.
(9) Hecht, C.; Stadler, F.; Schmidt, P. J. S.; Günne, J. S.; Baumann, V.; Schnick, W. *Chem. Mater.* **2009**, *21*, 1595−1601.
(10) Wilson, M. A.; McCarthy, S. A. *Anal. Chem.* **1985**, *57*, 2733−2735.
(11) Boultif, A.; Louer, D. *J. Appl. Crystallogr.* **2004**, *37*, 724−731.
(12) Toby, B. H. *J. Appl. Crystallogr.* **2001**, *34*, 210−213.
(13) Hollerman, W. A.; Allison, S. W.; Goedeke, S. M.; Boudreaux, P.; Guidry, R.; Gates, E. *IEEE Trans. Nucl. Sci.* **2003**, *50*, 754−757.
(14) Dorenbos, P. *J. Lumin.* **2003**, *104*, 239−260.
(15) Setlur, A. A.; Heward, W. J.; Gao, Y.; Srivastava, A. M.; Chandran, R. G.; Shankar, M. V. *Chem. Mater.* **2006**, *18*, 3314−3322.
(16) Tomiki, T.; Kohatsu, T.; Shimabukuro, H.; Ganaha, Y. *J. Phys. Soc. Jpn.* **1992**, *61*, 2382−2387.
(17) Liu, Y.; Zhang, X.; Hao, Z.; Lu, W.; Liu, X.; Wang, X.; Zhang, J. *J. Phys. D: Appl. Phys.* **2011**, *44*, 075402-1−075402-6.
(18) Zeuner, M.; Pagano, S.; Schnick, W. *Angew. Chem. Int. Ed.* **2011**, *50*, 7754−7775.
(19) Schlieper, T.; Milius, W.; Schnic, W. *Z. Anorg. Allg. Chem.* **1995**, *621*, 1380−1384.
(20) Höppe, H. A.; Lutz, H.; Morys, P.; Schnick, W.; Seilmeier, A. *J. Phys. Chem. Solids* **2000**, *61*, 2001−2006.
(21) Sohn, K. S.; Lee, S.; Xie, R. J.; Hirosaki, N. *Appl. Phys. Lett.* **2009**, *95*, 121903-1−121903-3.
(22) Brown, I. D.; Altermatt, D. *Acta Crystallogr., Sect. B* **1985**, *41*, 244−247.
(23) Ottinger, F.; Kroslakova, I.; Hametner, K.; Reusser, E.; Nesper, R.; Günther, D. *Anal. Bioanal. Chem.* **2005**, *383*, 489−499.
(24) Kechele, J. A.; Hecht, C.; Oeckler, O.; Jörn, S. G.; Peter, J. S.; Wolfgang, S. *Chem. Mater.* **2009**, *21*, 1288−1295.
(25) Pilet, G.; Grins, J.; Edén, M.; Esmaeilzadeh, S. *Eur. J. Inorg. Chem.* **2006**, *18*, 3627−3633.
(26) Piao, X.; Machida, K.; Horikawa, T.; Hanzawa, H.; Shimomura, Y.; Kijima, N. *Chem. Mater.* **2007**, *19*, 4592−4599.
(27) Dorenbos, P. *Phys. Rev. B* **2000**, *62*, 15640−15649.
(28) Krevel, J. W. H.; Hintzen, H. T.; Metselaar, R. *Mater. Res. Bull.* **2000**, *35*, 747−754.
(29) Brown, A. L.; Norton, M. G. *J. Mater. Sci. Lett.* **1998**, *17*, 1519−1522.

(30) Liu, Y.; Zhang, X.; Hao, Z.; Wang, X.; Zhang, J. *J. Mater. Chem.* **2011**, *21*, 6354−6358.
(31) Sohn, K. S.; Kwak, J. H.; Jung, Y. S.; Yan, H.; Reece, M. J. *J. Electrochem. Soc.* **2008**, *155*, J58−J61.